Materials Science and Engineering C 59 (2016) 500–508

Contents lists available at ScienceDirect

Materials Science and Engineering C

journal homepage: www.elsevier.com/locate/msec

Synthesis and characterization of Co_3O_4 ultra-nanosheets and Co_3O_4 ultra-nanosheet-$Ni(OH)_2$ as non-enzymatic electrochemical sensors for glucose detection

M.R. Mahmoudian [a,b,*], W.J. Basirun [a], Pei Meng Woi [a], M. Sookhakian [c], Ramin Yousefi [d], H. Ghadimi [a], Y. Alias [a,**]

[a] Department of Chemistry, University of Malaya, Kuala Lumpur 50603, Malaysia
[b] Department of Chemistry, Shahid Sherafat, University of Farhangian, 15916 Tehran, Iran
[c] Department of Physics, University of Malaya, Kuala Lumpur 50603, Malaysia
[d] Department of Physics, Masjed-Soleiman Branch, Islamic Azad University (I.A.U), Masjed-Soleiman, Iran

ARTICLE INFO

Article history:
Received 10 May 2015
Received in revised form 2 October 2015
Accepted 15 October 2015
Available online 19 October 2015

Keywords:
Glucose
Biosensor
Non-enzymatic sensing
Electrochemical sensing

ABSTRACT

The present study examines the synthesis of Co_3O_4 ultra-nanosheets (Co_3O_4 UNSs) and Co_3O_4 ultra-nanosheet-$Ni(OH)_2$ (Co_3O_4 UNS-$Ni(OH)_2$) via solvothermal process and their application as non-enzymatic electrochemical sensors for glucose detection. X-ray diffraction and transmission electron microscopy results confirmed the Co_3O_4 UNS deposition on $Ni(OH)_2$ surface. The presence of Co_3O_4 UNSs on Ni $(OH)_2$ surface improved the sensitivity of glucose detection, from the increase of glucose oxidation peak current at the Co_3O_4 UNS-$Ni(OH)_2$/glassy carbon electrode (current density: 2000 $\mu A \cdot cm^{-2}$), compared to the Co_3O_4 UNSs. These results confirmed that $Ni(OH)_2$ on glassy carbon electrode is a sensitive material for glucose detection, moreover the Co_3O_4 UNSs can increase the interaction and detection of glucose due to their high surface area. The estimated limit of detection (S/N = 3) and limit of quantification (S/N = 10) of the linear segment (5–40 μM) are 1.08 μM and 3.60 μM respectively. The reproducibility experiments confirmed the feasibility of Co_3O_4 UNS-$Ni(OH)_2$ for the quantitative detection of certain concentration ranges of glucose.

1. Introduction

The main research focus in glucose detection is the development of a stable and sensitive non-enzymatic electrochemical sensor due to the intrinsic problems associated with enzymes. Sensitive and selective glucose sensors are important in different applications [1]. Determination of these factors is not only relevant for applications in blood sugar monitoring, but also in the food industry, bio-processing and in the development of renewable, sustainable fuel cells [2]. The application of non-enzymatic electrode for the direct oxidation of glucose gives greater sensitivity, with oxidation currents as high as mA cm^{-2} [2,3]. However, the superior selectivity and relative non-toxicity of enzyme based electrodes are the focus of commercially available glucose sensors. Recent investigations have shown that the development of non-enzymatic electrochemical glucose sensors utilizing Pt and Ag resulted in the poisoning by the adsorbed intermediates which led to lower sensitivities [4,5]. Moreover, the presence of common interference such as ascorbic acid (AA) and uric acid (UA) decreases the accuracy of glucose detection at these electrodes [6].

In recent years, scientists have focused more attention to the organization of nanostructures, transcending new dimensions for the design of functional materials [7–9]. Recent reports have shown that materials with the same composition but different morphologies exhibit different properties which are suitable for a wide range of applications [10,11]. The increase of the available surface area enhances the ability of the composites to interact with other materials, are one of the main advantage of this type of material. Cobalt oxide (Co_3O_4), an eco-friendly material with favorable capacitive characteristics, is a suitable material for a wide range of applications such as supercapacitors, sensors, heterogeneous catalysts and magnetic materials [12–14]. NiO and $Ni(OH)_2$ are other materials which can be used in glucose detection [15], NiO is an efficient catalyst for glucose electro-oxidation in alkaline medium, due to the absence of poisoning from reactive intermediates in solution [16]. Yu Lei et al. [17] fabricated NiO–Pt nanofibers using a two-step method, and obtained improved sensitivity of glucose detection, the presence of Pt nanoparticles. Cao et al. [18] reported a method to synthesize different morphologies of Co_3O_4 with a highly ordered superstructure. They obtained various shapes of Co_3O_4, such as simple

* Correspondence to: M.R. Mahmoudian, Department of Chemistry, University of Malaya, Kuala Lumpur 50603, Malaysia.
** Corresponding author.
E-mail addresses: M_R_mahmoudian@yahoo.com (M.R. Mahmoudian), Yatimah70@um.edu.my (Y. Alias).

http://dx.doi.org/10.1016/j.msec.2015.10.055
0928-4931/

nanoplates to well-organized cabbage-like structures, and confirmed the influence of morphology on the detection of certain analytes. Therefore, the synthesis of Co_3O_4 nanocomposites with the incorporation of NiO or $Ni(OH)_2$ as a non-enzymatic glucose sensor is an interesting approach, due to the ability of nanoscale Co_3O_4 to exist in different morphologies, which may influence its detection sensitivity. In this work, we report the synthesis of Co_3O_4 UNSs and Co_3O_4 UNS-$Ni(OH)_2$ via the solvothermal method and their applications as non-enzymatic glucose electrochemical sensors.

2. Experimental methods

2.1. Synthesis of Co_3O_4 UNS-$Ni(OH)_2$ and Co_3O_4 UNSs

The $CoSO_4 \cdot 7H_2O$, Ni power, D-(+) glucose, Cobalt (II,III) oxide powder (<10 μm), and hexadecyl trimethyl ammonium bromide (CTAB) were procured from Sigma-Aldrich (St. Louis, Mo, USA). All chemical reagents were of analytical grade and used as received. In a typical process, 1.5 g $CoSO_4 \cdot 7H_2O$ was dissolved in a mixture of water (6 ml), methanol (36 ml) and 1.5 g of CTAB, and stirred for 20 min until the solution turned red. The solution was then transferred into a 60 ml Teflon-lined stainless steel autoclave. Nickel powder (0.08 g) was then added into the solution and autoclaved at 170 °C for 24 h in the solvothermal process. When the reaction was complete, the autoclave was cooled to room temperature; the precipitates were filtered and washed with distilled water to remove the excess reagents. In the final step, the samples were calcined at 250 °C for 4 h. The synthesis of Co_3O_4 UNSs was repeated in the absence of Ni powder, to investigate the influence of $Ni(OH)_2$ on the morphology and sensing performance of the Co_3O_4 UNSs in glucose detection. Moreover, to understand the influence of $Ni(OH)_2$ on glucose detection, the synthesis process was repeated in the absence of $CoSO_4 \cdot 7H_2O$.

2.2. Fabrication of the glucose sensor

The synthesized Co_3O_4 UNSs, Co_3O_4 UNS-$Ni(OH)_2$, mixture of Cobalt (II,III) oxide (micro-size)/$Ni(OH)_2$ (ratio 1:1), Cobalt (II,III) oxide (micro-size) and $Ni(OH)_2$ were dispersed separately (1 mg) in DMF (1 ml) with ultra-sonication for 10 min, to obtain a homogenous suspension. Then, 5 μl of the homogenous suspension was dropped on polished glassy carbon electrode (GCE) surface and dried at room temperature.

2.3. Instruments

Transmission electron microscopy (TEM) (Philips CM200, at an operating voltage of 200 kV) was used to investigate the morphology of the Co_3O_4 UNSs and Co_3O_4 UNS-$Ni(OH)_2$. X-ray diffraction (Siemens D5000, Cu Kα radiation) was used to analyze the crystalline structure of the powders. Electrochemical impedance spectroscopy (EIS) measurements were performed in 1 mM $Fe(CN)_6^{3-/4-}$ (1:1) solution in 0.1 M KCl supporting electrolyte. The impedance spectra were obtained over a frequency range of 100 kHz–0.1 Hz, with an acquisition of 10 points per decade and signal amplitude of 5 mV around the open circuit potential. The analysis of the impedance spectra was performed by fitting the experimental results to equivalent circuits using the non-linear least-square fitting procedure. A potentiostat/galvanostat model PGSTAT-302N from Autolab (Ecochemie, Netherlands), controlled by a USB IF030 (Metrohm Autolab) interface card with the FRA.EXE software (version: 409.007, distributor: Metrohm Malaysia) installed in a PC was used to perform these experiments. A glassy carbon electrode (GCE), Ag/AgCl and a platinum wire (Pt) were the working, reference and counter electrodes, respectively and the current density was used instead of current. UV–vis spectroscopy (Shimadzu, Japan) was used to determine the concentration of glucose in solution. The wavelength was scanned from 190 to 400 nm to determine the presence of glucose.

3. Results and discussions

3.1. Characterization of Co_3O_4 UNSs and Co_3O_4 UNS-$Ni(OH)_2$

3.1.1. TEM and selective area electron diffraction (SAED) pattern

The TEM images of Co_3O_4 UNSs and Co_3O_4 UNS-$Ni(OH)_2$ are shown in Fig. 1(a), (b) and (c), (d), respectively. The results clearly show two different morphologies of Co_3O_4 where most of them are in the ultra-hexagonal nanosheet form (Fig. 1(a)). Moreover, a higher magnification of the TEM image (Fig. 1(b)) confirms the transparent state of the synthesized Co_3O_4 UNSs. The ultra-nanosheet morphology of the Co_3O_4 provides a large surface area for greater sensitivity and faster reaction with the analyte. The TEM images of the Co_3O_4 UNS-$Ni(OH)_2$ with a lower and higher magnification are shown in Fig. 1(c) and (d), respectively. The result confirms a homogenous ultra-nanosheet morphology of the Co_3O_4 deposited on the $Ni(OH)_2$ surface. Moreover, the TEM images reveal that the size of Co_3O_4 UNSs deposited on $Ni(OH)_2$ has decreased compared to Co_3O_4 UNSs in the absence of $Ni(OH)_2$, thus the deposited Co_3O_4 UNSs have larger surface area. Selective area electron diffraction (SAED) patterns of Co_3O_4 UNSs and Co_3O_4 UNS-$Ni(OH)_2$ are shown in Fig. 1(e) and (f) respectively. The SAED pattern of Co_3O_4 UNSs reveals a polycrystalline phase but shows two separated phases which belongs to Co_3O_4 UNSs and $Ni(OH)_2$, for the Co_3O_4 UNS-$Ni(OH)_2$.

3.1.2. The XRD results

The XRD patterns of Co_3O_4 UNSs and Co_3O_4 UNS-$Ni(OH)_2$ are shown in Fig. 2(a) and (b) respectively. Fig. 2(a) shows the intensity for the (1 1 1), (2 2 0), (311), (222), (400) (331), (422) (511) and (440) peaks which are attributed to Co_3O_4 (XRD Ref. code: 01-073-1701). The XRD results confirm that Co^{2+} was converted to Co_3O_4 UNSs during the solvothermal process. The XRD result in Fig. 2(b) confirms the presence of Co_3O_4 UNS-$Ni(OH)_2$. The peaks marked with (♦) are attributed to $Ni(OH)_2$ ((006), (009), (105), (107), (1010) and (0014), ref. code: (00-006-0044)) in Fig. 2(b). The XRD result confirms that the Ni powder was oxidized to Ni^{2+}. Therefore, from the XRD and TEM results, the synthesis of Co_3O_4 UNSs in the presence of Ni powder resulted in the decrease of the size of Co_3O_4 UNSs. The Ni powder was also oxidized to Ni^{2+}, and the presence of Ni^{2+} enhanced the sensitivity of glucose detection [19]. Moreover, the TEM images show the agglomeration of Co_3O_4 UNSs on the $Ni(OH)_2$ surface, which is a major disadvantage of this synthetic method. The effect of the particle size on the sensitivity of glucose detection will be discussed in the next section. Moreover, the XRD patterns indicate that the Co_3O_4 is a single phase with polycrystalline structure, while the Co_3O_4-$Ni(OH)_2$ is a dual-phase polycrystalline structure. In addition, greater brightness of the Co_3O_4 spots reveals a higher degree of crystallinity compared to the Co_3O_4-$Ni(OH)_2$. In fact, the XRD patterns are in good agreement with SAED patterns.

3.1.3. EIS results

The interfacial properties of the GCE electrodes modified with Co_3O_4 UNSs and Co_3O_4 UNS-$Ni(OH)_2$ were studied by EIS. Fig. 3(a) and (b) shows the Nyquist and Bode plots of (1) Co_3O_4 UNS-$Ni(OH)_2$/GCE, (2) Co_3O_4 UNSs/GCE and (3) bare GCE and their equivalent circuits in 1 mM $Fe(CN)_6^{3-/4-}$ (1:1) in 0.1 M KCl supporting electrolyte. The Nyquist plots of all three electrodes show large semicircles which are due to the high interfacial resistance (R_{ct}). The behaviors of Co_3O_4 UNS-$Ni(OH)_2$/GCE and Co_3O_4 UNSs/GCE are similar to the bare GCE but have semicircles with smaller diameters. The Nyquist plots indicate a "depressed semi-circle" with the center of the circle below the Z_R axis, which is due to the deviation from the double layer capacitance. A constant phase element (CPE) was introduced instead of a pure capacitor in the fitting procedure to obtain a good agreement between the simulated and experimental data. The impedance of CPE is defined as $Z_{CPE} = Q^{-1}(j\omega)^{-n}$; where Q is the combination of properties related to the surface and electroactive species independent of frequency; "n" is related to the

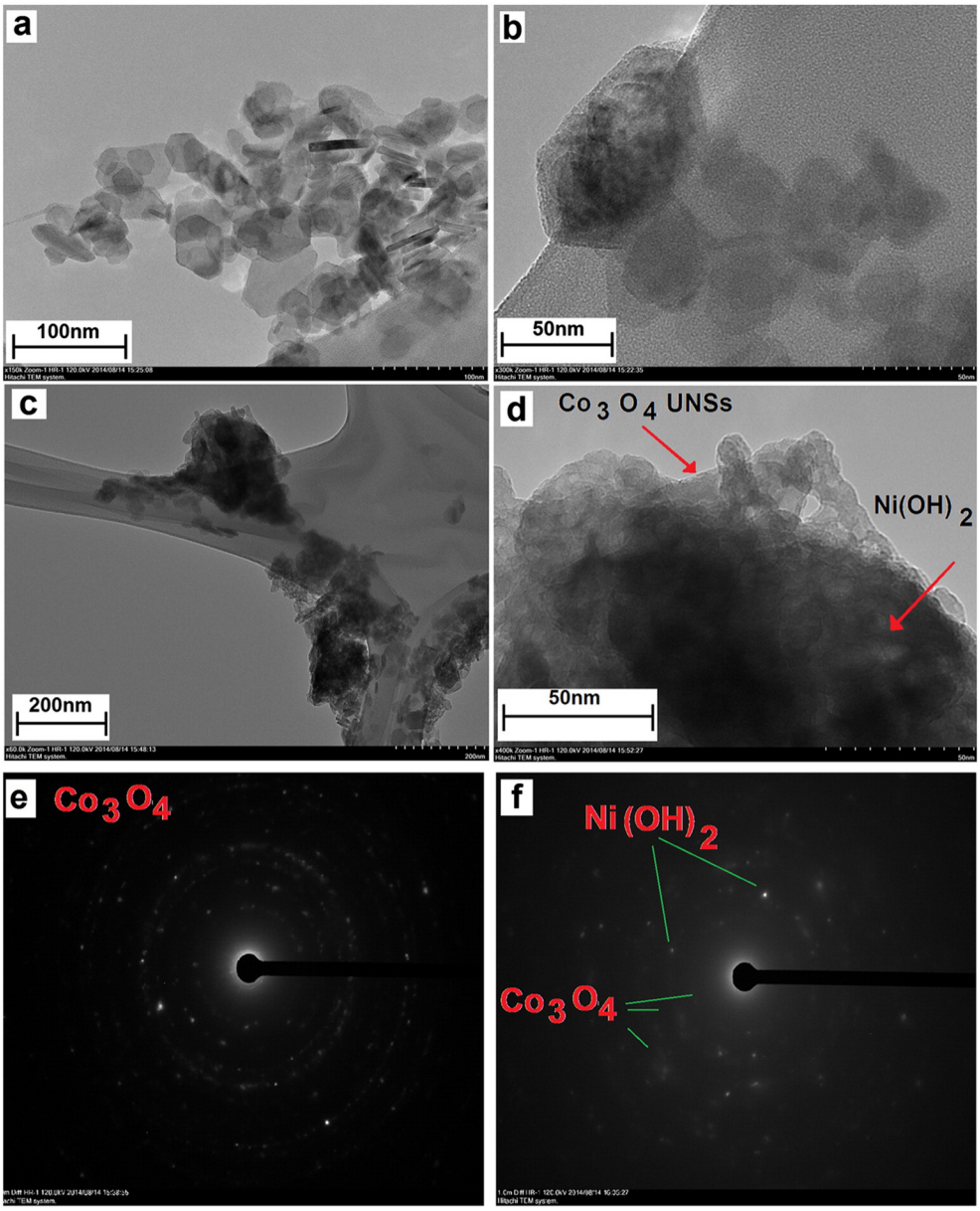

Fig. 1. TEM images of: (a, b) Co_3O_4 UNSs and (c, d) Co_3O_4 UNS-$Ni(OH)_2$. (e) The selective area electron diffraction patterns of (e) Co_3O_4 UNSs and (f) Co_3O_4 UNS-$Ni(OH)_2$.

slope of the log *Z* vs. log *f*. The parameters obtained by the simulation of the EIS results of Co_3O_4 UNS-$Ni(OH)_2$/GCE and Co_3O_4 UNSs/GCE confirm the influence of $Ni(OH)_2$ on the decrease of R_{ct} (Table 1). The equivalent circuit diagram of Co_3O_4 UNS-$Ni(OH)_2$/GCE and Co_3O_4 UNSs/GCE (Fig. 3(a) and Table 1) shows that the capacitance (CPE) is parallel with the R_{ct} which is due to the pore formation on the electrode surface. The decrease of CPE (*Q*) from Co_3O_4 UNSs/GCE to Co_3O_4 UNS-$Ni(OH)_2$/GCE is attributed to the agglomeration phenomenon, which decreases the size of the Co_3O_4 UNSs deposited on the $Ni(OH)_2$ surface. Surface roughness has a large influence to the CPE behavior. The fractal dimension (D) is around 2–3 for a rough surface. The electrode surface can be considered between 2 dimensions (flat) and 3 dimensions (similar to a porous cube). Other researchers believe that for these type of electrodes, the interfacial impedance is modified by an exponent, $n = 1/(D-1)$ [20]. For a smooth surface, the fractal dimension (D) is 2.0 and $n = 1$, while for a highly contorted surface, D is 3 and $n = 0.5$. The decrease of "*n*" from Co_3O_4 UNSs/GCE to Co_3O_4 UNS-$Ni(OH)_2$/GCE shows an increase in the surface roughness. The increase in surface roughness increases the available surface area, which is one of the objectives of the electrode fabrication. Each parallel R_{ct} element is represented by a semicircle with a diameter smaller than the R_{ct} of Co_3O_4 UNSs/GCE, which is due to a much faster interfacial electron transfer process and higher conductivity of the electrochemical sensing platform. The effect of $Ni(OH)_2$ is confirmed by the Bode plots in Fig. 3(b). The comparison of log |*Z*| of all three electrodes shows that the charge transfer resistance has decreased significantly with the presence of $Ni(OH)_2$.

3.2. The performance of Co_3O_4 UNSs and Co_3O_4 UNS-$Ni(OH)_2$ modified GCE in the detection of glucose

Fig. 4(a) shows the cyclic voltammograms of Co_3O_4 UNS-$Ni(OH)_2$/GCE (1), Co_3O_4 UNSs/GCE (2), $Ni(OH)_2$/GCE (3) and bare GCE (5) in the presence of 1.0 mM glucose, and Co_3O_4 UNS-$Ni(OH)_2$/GCE in the absence of glucose (4) in 0.1 M NaOH. The inset of Fig. 4 shows the comparison of the cyclic voltammogram of Co_3O_4 UNS-$Ni(OH)_2$/GCE (1) with modified GCE with Co_3O_4 micro-size (>10 μm) and modified GCE with the mixture of Co_3O_4 micro-size/$Ni(OH)_2$ (with ratio of 1:1)

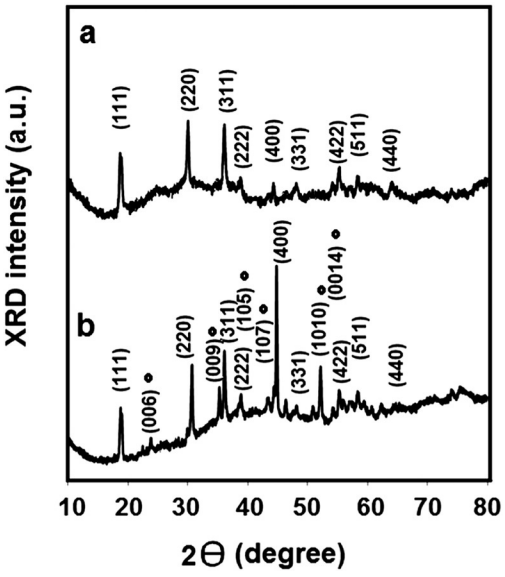

Fig. 2. XRD pattern of: (a) Co_3O_4 UNSs and (b) Co_3O_4 UNS-$Ni(OH)_2$.

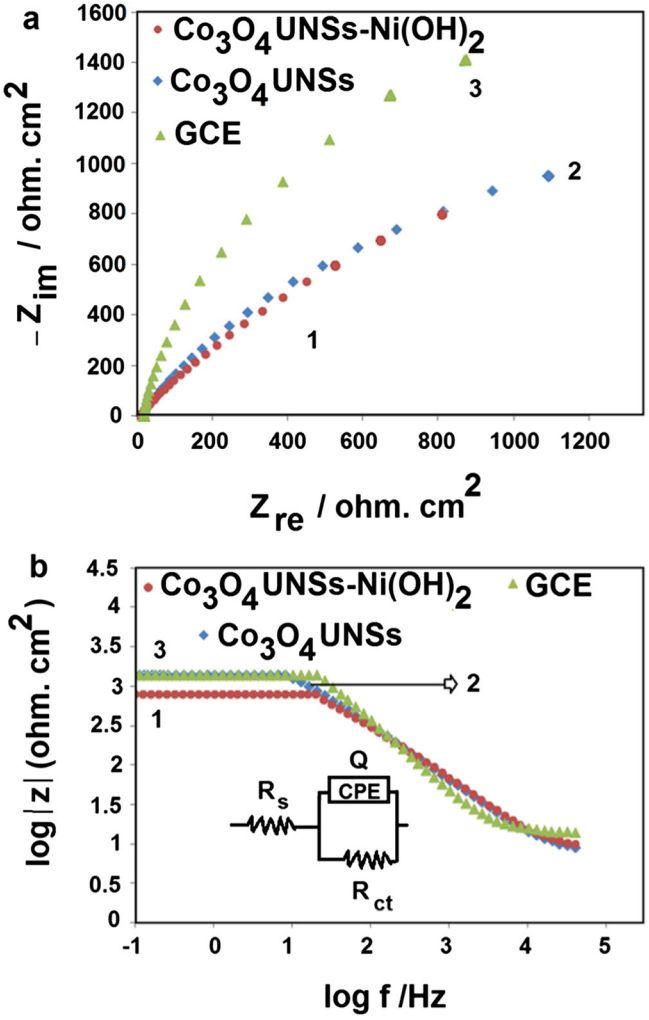

Fig. 3. (a) Nyquist and (b) Bode plots of (1) Co_3O_4 UNS-$Ni(OH)_2$/GCE, (2) Co_3O_4 UNS/GCE and (3) bare GCE and their equivalents circuits in 0.1 M KCl solution containing 1 mM $Fe(CN)_6^{3-/4-}$ (1:1).

Table. 1
Electrochemical parameters obtained by simulation of the EIS results on the GCE, Co_3O_4 UNSs and Co_3O_4 UNS-$Ni(OH)_2$ in a 0.1 M KCl solution containing 1 mM $Fe(CN)_6^{3-/4-}$ (1:1).

Electrode	R_1 (R_s) Ohm·cm^2	R_2 (R_{ct}) kOhm·cm^2	Q Y (mOhm^{-1}·s^n cm^{-2})	n
GCE	5.73	1.789	0.01215	0.8661
Co_3O_4 NUS/GCE	5.81	1.551	0.03235	0.7112
Co_3O_4 NUS/nickel oxide hydroxide/GCE	5.78	0.824	0.04147	0.6814

in the presence of 1.0 mM glucose and 0.1 M NaOH (scan rate: 50 mV s^{-1}). The Co_3O_4 UNS-$Ni(OH)_2$/GCE shows good response and improved performance for the oxidation of glucose compared to Co_3O_4 UNSs/GCE and $Ni(OH)_2$/GCE, and is consistent with previous report [21]. The increase of the oxidation peak current to more than 1800 μA·cm^{-2} and the shift of the oxidation peak potential to lower than 0.4 V confirm the high sensitivity of this electrode for glucose detection. There are two reasons for the improved catalytic performance of the Co_3O_4 UNS-$Ni(OH)_2$ compared to Co_3O_4 UNSs and $Ni(OH)_2$/GCE. First, the size of the Co_3O_4 UNSs deposited on the $Ni(OH)_2$ surface is smaller than the Co_3O_4 UNSs synthesized without the $Ni(OH)_2$, thus the available surface area is increased and the agglomeration phenomenon could not significantly influence the reaction of the deposited Co_3O_4 UNSs with glucose. Second, the presence of $Ni(OH)_2$ could improve the performance of the Co_3O_4 UNS-$Ni(OH)_2$/GCE for the detection of glucose. From the comparison of the oxidation peak potential in plots (1) and (2), the oxidation peak of Co_3O_4 UNS-$Ni(OH)_2$/GCE is shifted to more positive region with the presence of $Ni(OH)_2$, which is consistent with previous reports [15,19]. In addition, from the comparison of plot (1) with plots (2) and (3), the synergistic effect of the $Ni(OH)_2$ and Co_3O_4 UNSs on the current response of the modified electrode with Co_3O_4 UNS-$Ni(OH)_2$/GCE toward glucose oxidation can be observed in Fig. 4. The possible mechanisms for the direct electrochemical oxidation of glucose can be given in the following equations [19,20]:

$$Co_3O_4\,UNSs + OH^- + H_2O \longrightarrow 3\,CoOOH + e^- \quad (1)$$

$$CoOOH + OH^- \longrightarrow CoO_2 + H_2O + e^- \quad (2)$$

$$CoO_2 + \text{glucose} \longrightarrow CoOOH + \text{glucolactone} \quad (3)$$

$$Ni(OH)_2 + OH^- \longrightarrow NiOOH + H_2O + e^- \quad (4)$$

$$NiOOH + \text{glucose} \longrightarrow Ni(OH)_2 + \text{glucolactone}. \quad (5)$$

Initially, the Co_3O_4 and $Ni(OH)_2$ are oxidized to CoOOH and NiOOH, as in Eqs. (1) and (4) respectively. This is followed by the further oxidation of CoOOH to CoO_2. The increase of the oxidation peak current is due to the reaction between NiOOH, CoO_2 and glucose, where the glucose is oxidized to glucolactone simultaneously, however the uncoated GCE shows no signs of the glucose oxidation peak (Scheme 1). Moreover, the results clearly show the effect of nanostructured materials on the sensitivity of glucose detection (inset of Fig. 4(a)). The increase of the Co_3O_4 UNS-$Ni(OH)_2$/GCE (1) peak current is much higher than the fabricated electrodes of Cobalt (II,III) oxide (micro-size)/$Ni(OH)_2$ (ratio 1:1) (2) and Cobalt (II,III) oxide (micro-size) (3) (inset of Fig. 4(a)), which suggests a superior catalytic activity of Co_3O_4 UNS-$Ni(OH)_2$/GCE toward glucose oxidation. This is due to the morphology of Co_3O_4 UNS-$Ni(OH)_2$ which not only offers larger space for ion diffusion, but also increases the availability of the catalytic material for glucose oxidation.

Fig. 4(b) shows the CVs of Co_3O_4 UNS-$Ni(OH)_2$/GCE at different scan rates with 1 mM glucose in 0.1 M NaOH. The linear increase of the oxidation peak current with scan rate shows that the electrode reaction of the immobilized $Ni(OH)_2$/NiOOH redox couple is a surface-confined

electrochemical process. The linear regression equation can be expressed as $I_{pa} = 25.74\upsilon\ (mV\ s^{-1}) + 28.81 (R^2 = 0.993)$ (Fig. 4(c)). Moreover, the almost linear relationship of I_{pa} and $v^{1/2}$ shows that the redox reaction is also a diffusion-controlled process, due to the presence of OH^- diffusion between the supporting electrolyte and the electrode surface (Fig. 4(d)). Due to the diffusion controlled process of the OH^-, the redox reactions on the electrode surface (Eqs. (1) and (4)), are also rate limiting, which limit the reactions (3) and (5) [22–26]. Therefore, the reaction on the electrode surface is basically a diffusion controlled process.

The dependency of the amperometric response on the applied potential of Co_3O_4 UNS-$Ni(OH)_2$/GCE under batch conditions was estimated over a potential range of 0.25 V to 0.50 V (Fig. 5(a)), in 1.0 mM glucose and 0.1 M NaOH (scan rate: 50 $mV \cdot s^{-1}$). An appropriate working potential was selected based on the least positive potential with good selectivity, and also a potential with a large analyte-dependent current. Fig. 6 indicates that 0.35 V fulfills these conditions; therefore, it was chosen as the working potential. A comparison of the selected working potential of this work with previous reports [27–28] shows a significant decrease in the applied potential of the working electrode,

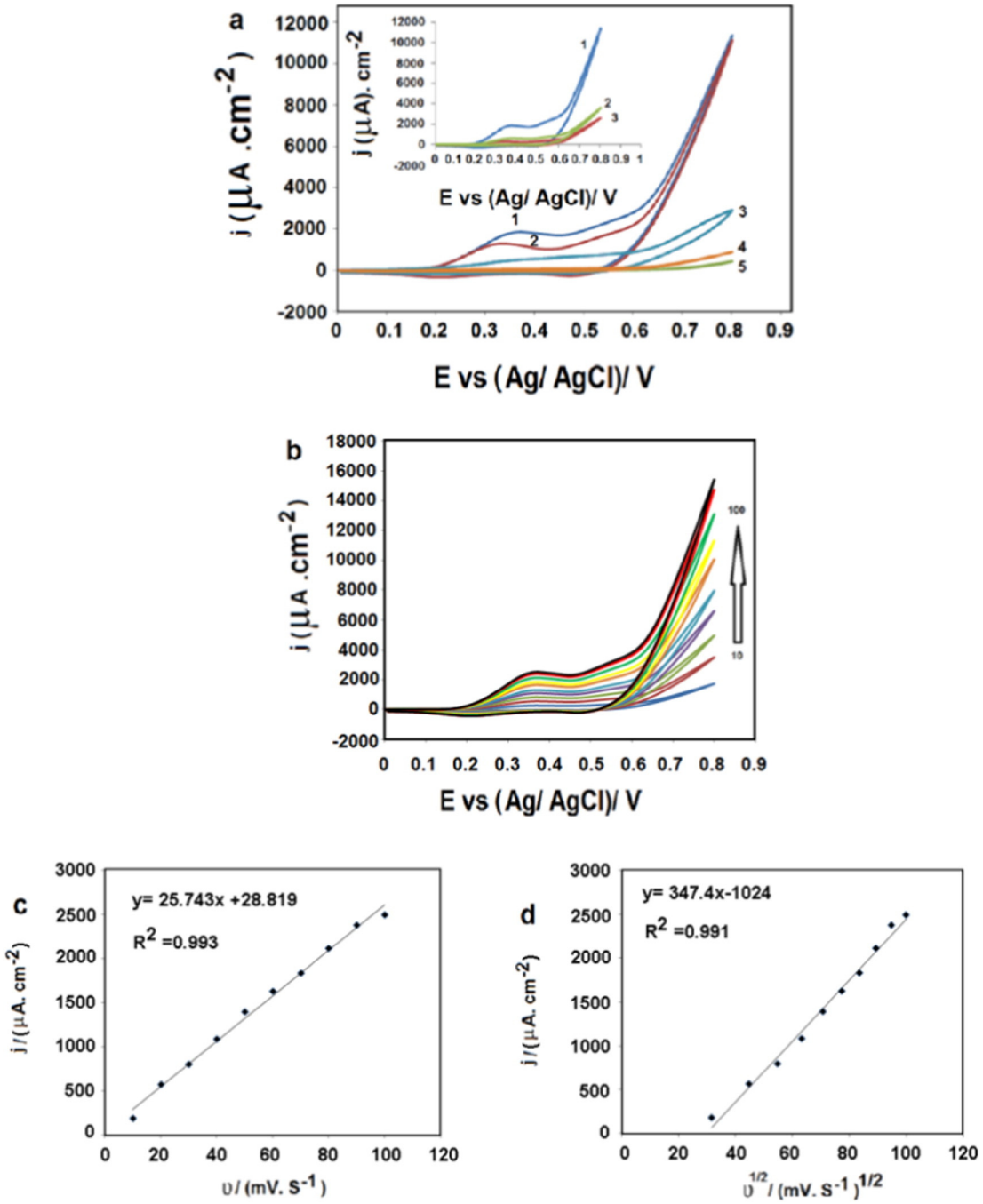

Fig. 4. (a) Cyclic voltammograms of: Co_3O_4 UNS-$Ni(OH)_2$/GCE (1), Co_3O_4 UNS/GCE (2), $Ni(OH)_2$/GCE (3) and bare GCE (5) in the presence of 1.0 mM glucose and 0.1 M NaOH (scan rate: 50 $mV \cdot s^{-1}$). Co_3O_4 UNS-$Ni(OH)_2$/GCE in the absence of glucose (4) in 0.1 M NaOH (scan rate: 50 $mV \cdot s^{-1}$). (inset: Co_3O_4 UNS-$Ni(OH)_2$/GCE (1), modified GCE with the mixture of Cobalt (II,III) oxide (micro-size)/$Ni(OH)_2$ (ratio 1:1) (2) and Cobalt (II,III) oxide (micro-size)/GCE (3) in the presence of 1.0 mM glucose and 0.1 M NaOH, scan rate: 50 mV s^{-1}. (b) The influence of scan rate on the peak current density of Co_3O_4 UNS-$Ni(OH)_2$/GCE. (c) The plot of anodic peak current density ($\mu A \cdot cm^{-2}$) vs. scan rate (mV s^{-1}): 10, 20, 30, 40, 50, 60, 70, 80, 90 and 100 in the presence of 1.0 mM glucose and 0.1 M NaOH. (d) The plot of anodic peak current density ($\mu A \cdot cm^{-2}$) vs. scan rate (mV $s^{-1})^{1/2}$ in the presence of 1.0 mM glucose and 0.1 M NaOH.

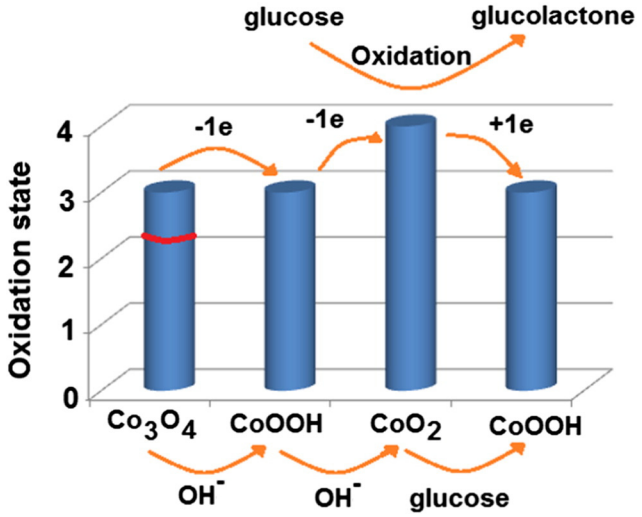

Scheme 1. The oxidation states of different species of oxide and hydroxide of Co for glucose oxidation.

which is one of the advantage of Co_3O_4 UNS-Ni$(OH)_2$/GCE in glucose detection.

The amperometric response of Co_3O_4 UNS-Ni$(OH)_2$/GCE toward the addition of glucose aliquots in 0.1 M NaOH was also performed and shown in Fig. 5(b). The responses were rapid, within 5 s. The current increases with the concentration of glucose between 5 and 200 μmol l^{-1}. The calibration curve for the Co_3O_4 UNS-Ni$(OH)_2$/GCE shows two linear segments: the first linear segment increases from 5 to 40 μM with a linear regression equation of $I = 1.089$ (μA μM^{-1} cm^{-2})–5.299 ($R^2 = 0.991$) (Fig. 5(c)), while the second linear segment increases up to 200 μM with a linear regression equation of $I = 2.145$ (μA μM^{-1} cm^{-2})–30.980 ($R^2 = 0.992$) (Fig. 5(d)). The limit of detection (LOD) and limit of quantification (LOQ) of Co_3O_4 UNS-Ni$(OH)_2$/GCE were calculated from the following equations: [29].

$$LOD = 3S_B/b \quad (6)$$

$$LOQ = 10S_B/b \quad (7)$$

where S_B is the standard deviation of the blank solution and b is the slope of the analytical curve, as shown in Fig. 5(c) and (d). The estimated LOD

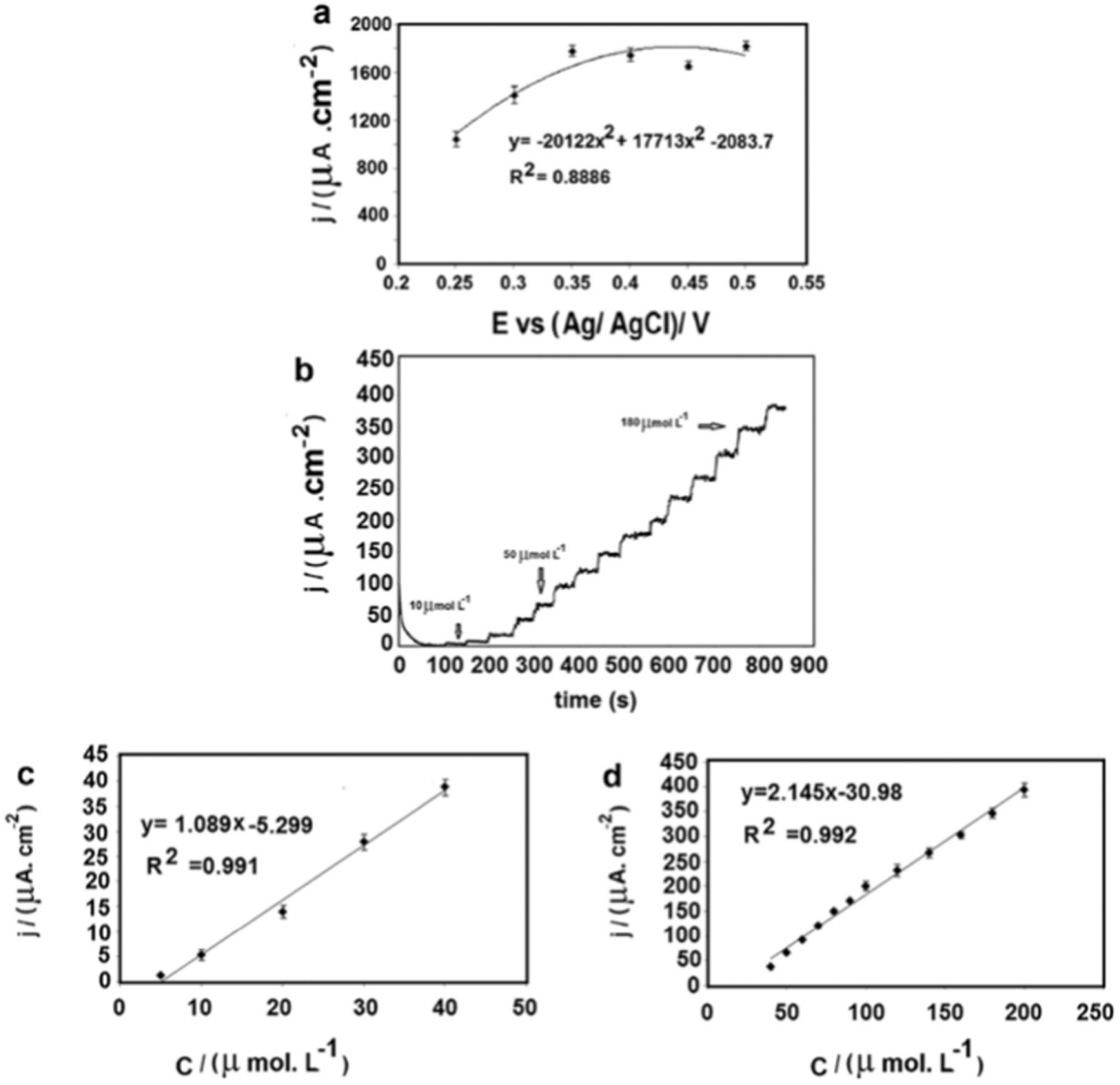

Fig. 5. (a) Effects of applied potential on the current density response of Co_3O_4 UNS-Ni$(OH)_2$/GCE to 1.0 mM glucose and 0.1 M NaOH. (b) Steady-state response of Co_3O_4 UNS-Ni$(OH)_2$/GCE to successive injections of glucose in 0.1 M NaOH with an applied potential of 0.35 V. (c) The calibration curve from 5 to 40 μM. (d) The calibration curve from 40 to 200 μM. Error bars represent ± standard deviation.

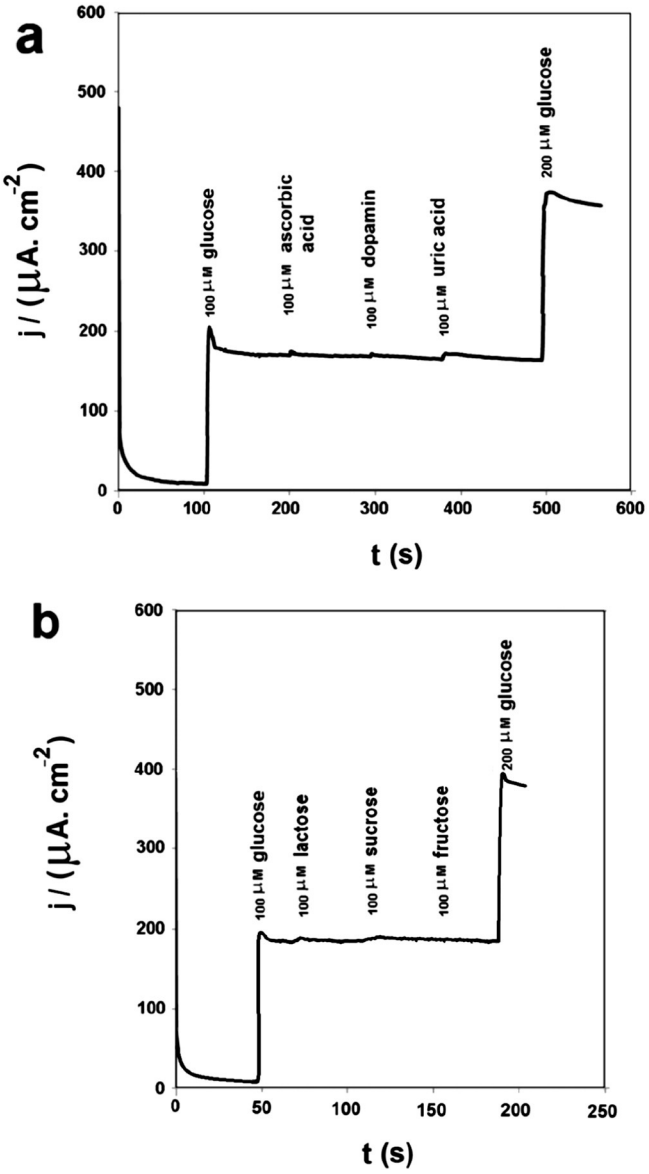

Fig. 6. (a) Current density–time response of Co_3O_4 UNS-Ni(OH)$_2$/GCE upon successive addition of 100 μM glucose, 100 μM of ascorbic acid, dopamine, uric acid, 200 μM glucose in 0.1 M NaOH at 0.35 V. (b) Current density–time response of Co_3O_4 UNS-Ni(OH)$_2$/GCE upon successive addition of 100 μM glucose, 100 μM of lactose, sucrose, fructose, and 200 μM glucose in 0.1 M NaOH at 0.35 V.

(S/N = 3) and LOQ (S/N = 10) of linear segment (5–40 μM of glucose) are 1.08 μM and 3.60 μM respectively. In addition, the sensitivity is 1.089 μA μM^{-1} cm^{-2} (5–40 μM of glucose) for the linear segment.

Table 3
The detection of glucose concentration in test samples (results based on six replicate determinations per sample).

Sample	Added/μmol l^{-1}	Found/μmol l^{-1}	(RSD%) (n = 6)	(Recovery%)
1	10	9.9725	2.7725	99.35
2	100	99.8251	2.1658	99.82
3	200	200.1298	2.8183	100.06

From Table 2, the LOD of glucose for the Co_3O_4 UNS-Ni(OH)$_2$/GCE is lower than those obtained on NiMOFs (6.15 μmol l^{-1}) [37] and nanoscale Ni hydroxide modified with CILEa (6 μmol l^{-1}) [31] and is comparable to that of Cu–NiO/GCE (0.5 μmol l^{-1}) [27] indicating a favorable analytical performance of this electrochemical sensor.

For analytical applications, a recovery experiment was also carried out to examine the prospective use of the Co_3O_4 UNS-Ni(OH)$_2$/GCE. Three different concentrations of glucose (10, 100 and 200 μmol l^{-1}) were added in 0.1 M NaOH, kept at the optimum potential of 0.35 V. All measurements were performed six times (n = 6) and the average recoveries are listed in Table 3. The recoveries and relative standard deviation (RSD) results show the feasibility of the fabricated electrode for the quantitative detection of certain concentration ranges of glucose. Easily oxidized compounds such as ascorbic acid (AA), dopamine (DO) and uric acid (UA) (Fig. 6(a)) and some sugars such as lactose, sucrose and fructose (Fig. 6(b)) are usually found together with glucose. In addition, the presence of other carbohydrate compounds can influence the detection of glucose. Therefore, interference tests were also performed with the addition of 100 μM glucose, followed by the addition of 100 μM of AA, DO, UA, lactose, sucrose, fructose and 200 μM glucose in 0.1 M NaOH, respectively. The result shows that AA, DO, and UA in Fig. 6(a) and lactose, sucrose, and fructose in Fig. 6(b) have negligible interference on glucose detection. The result also confirms that the electrode surface remains stable and viable, and the depletion of glucose is the main reason for the decrease in the oxidation current. The modified electrode showed acceptable stability and the response remains stable, even after 10 continuous cycles (~89%) which indicates that the inhibition of glucose detection is absent. This is due to the ultra-nanosheet morphology of Co_3O_4 UNSs with a large surface area that increases the adhesion of materials on the surface of GCE. The high selectivity of Co_3O_4 UNS-Ni(OH)$_2$/GCE can be explained by the repelling effect. Co_3O_4 has an isoelectric point (IEP) of ~8 and is negatively charged in 0.1 M NaOH. The UA, AA and DO are also negatively charged due to the loss of protons in the presence of hydroxyl ions and phenolic groups. Therefore, the electrocatalytic oxidation of UA, AA and DO at Co_3O_4 UNS-Ni(OH)$_2$ is decreased by the charge repelling effect [32].

3.3. Analysis of real samples

The Co_3O_4 UNS-Ni(OH)$_2$/GCE has been utilized for glucose detection in a commercial green tea. All measurements were performed six times (n = 6). The results were compared with the standard method

Table 2
Summary and comparison of the estimated LOD and sensitivity range of the present work and previous reports.

Type of electrode	Electrolyte	Performance	Sensitivity	Linear range	Reference
		LOD/μmol l^{-1}	μA μM^{-1} cm^{-2}	μmol l^{-1}	
NiO–Pt NFs/GCE	0.1 M NaOH	0.31	0.18	100–6000	[17]
Cu–NiO/GCE	0.4 M NaOH	0.5	0.171	0.5–5000	[27]
CAT-NiO	PBS pH 7	0.6	0.159	1–1000	[30]
Nanoscale Ni hydroxide modified CILEa	0.5 M NaOH	6	0.202	50–2300	[31]
Co_3O_4–rGO nanocomposites	0.1 M NaOH	0.18	1.366	0.5–1277	[33]
PINA(SDS)/Ni(OH)$_2$ modified CPE	0.1 M NaOH	90	0.584	160–750	[34]
sG–Ni/NiO	0.1 M NaOH	0.28	0.482	0.1–5	[35]
NiO-HMS	0.1 M NaOH	0.53	2.39	1.67–420	[36]
NiMOFs	0.1 M NaOH	6.15	0.395	1.8–1200	[37]
Co_3O_4 UNS-Ni(OH)$_2$/GCE	0.1 M NaOH	1.08	1.089	5–40	This work

Table 4
Amperometric and UV–vis spectrometric determination of glucose in commercial beverage green tea.

Sample	Added (mM)	Amperometric measurements		UV–vis-spectrometric measurements			
		Founding (mM)	Recovery%	RSD% (n = 6)	Founding (mM)	Recovery%	RSD% (n = 6)
1	0.04	0.0403	100.58	3.2961	0.0399	99.38	0.2277
2	0.08	0.0794	99.27	2.2516	0.0802	100.32	0.7364
3	0.16	0.1594	99.67	3.5434	0.1600	100.00	0.7705

of UV–vis spectrometry (Table 4). The real sample was purchased and the concentration of glucose was determined by the standard addition method. This was achieved with the addition of 0.1 M NaOH solution to a fixed volume of real sample (1 ml) at the optimum potential of 0.35 V. The results are in good agreement with the data obtained from the reference method (standard UV–vis spectrometry).

4. Conclusions

Co_3O_4 ultra-nanosheets (Co_3O_4 UNSs) and Co_3O_4 ultra-nanosheet-$Ni(OH)_2$ (Co_3O_4 UNS-$Ni(OH)_2$) were synthesized via a solvothermal process, and the Co_3O_4 UNS-$Ni(OH)_2$ was utilized as a sensor for the detection of glucose. XRD and TEM results confirmed the presence of Co_3O_4 UNS-$Ni(OH)_2$ and the deposition of ultra-hexagonal transparent Co_3O_4 on the $Ni(OH)_2$ surface. The GCE coated with the Co_3O_4 UNS-$Ni(OH)_2$ gave the highest electrocatalytic activity compared to the modified GCE with Co_3O_4 UNSs. EIS results confirmed that the charge transfer resistance of the coated GCE with Co_3O_4 UNS-$Ni(OH)_2$ was decreased compared to the Co_3O_4 UNSs, which is attributed to the presence of $Ni(OH)_2$. The estimated limit of detection (S/N = 3) and limit of quantification (S/N = 10) of the linear segment (5–40 μM of glucose) are 1.08 μM and 3.60 μM respectively. The ultra-transparent Co_3O_4 deposited on $Ni(OH)_2$ surface provides the highest available surface area and lowest R_{Ct}, which are the principal reasons for its high performance in glucose detection. One of the main advantages of the fabricated Co_3O_4 UNS-$Ni(OH)_2$ in glucose detection is its high sensitivity, even in low positive potential regions.

Acknowledgments

The authors wish to thank Mojdeh Yeganeh for the valuable discussion. This research is supported by High Impact Research MoE Grant UM.C/625/1/HIR/MoE/SC/04 from the Ministry of Education Malaysia, UMRG Program RP012A-14SUS, PRGS grant PR002-2014A, FP033 2013A, GC001C-14SBS, and RP038C-15HTM and University Malaya Centre for Ionic Liquids (UMCiL).

References

[1] X. Zhou, X. Dai, J. Li, Y. Long, W. Li, Y. Tu, A sensitive glucose biosensor based on Ag@C core–shell matrix, Mater. Sci. Eng. C 49 (2015) 579–587.
[2] Q. Yi, W. Huang, W. Yu, L. Li, X. Liu, Hydrothermal synthesis of titanium-supported nickel nanoflakes for electrochemical oxidation of glucose, Electroanalysis 20 (2008) 2016–2022.
[3] E. Ghasemi, E. Shams, N. Farzin Nejad, Covalent modification of ordered mesoporous carbon with glucose oxidase for fabrication of glucose biosensor, J. Electroanal. Chem. 752 (2015) 60–67.
[4] L.Q. Rong, C. Yang, Q.Y. Qian, X.H. Xia, Study of the nonenzymatic glucose sensor based on highly dispersed Pt nanoparticles supported on carbon nanotubes, Talanta 72 (2007) 819–824.
[5] X.J. Bo, J.C. Ndamanisha, J. Bai, L.P. Guo, Nonenzymatic amperometric sensor of hydrogen peroxide and glucose based on Pt nanoparticles/ordered mesoporous carbon nanocomposite, Talanta 82 (2010) 85–91.
[6] W. Wang, L. Zhang, S. Tong, X. Li, W. Song, Three-dimensional network films of electrospun copper oxide nanofiber for glucose determination, Biosens. Bioelectron. 25 (2009) 708–714.
[7] H. Colfen, S. Mann, Higher-order organization by mesoscale self-assembly and transformation of hybrid nanostructures, Angew. Chem., Int. Ed. 42 (2003) 2350–2365.
[8] X. Sun, B. Zhu, Ding-Kun Ji, Q. Chen, xiao-peng he, Guo-rong Chen, T. D. James, Selective fluorescence detection of monosaccharides using a material composite formed between graphene oxide and boronate-based receptors, ACS Appl. Mater. Interfaces 6 (2014) 10078–10082.
[9] X.-P. He, B.-W. Zhu, Y. Zang, J. Li, G.-R. Chen, T. He, Y.-T. Long, Dynamic tracking of pathogenic receptor expression of live cells using pyrenyl glycoanthraquinone-decorated graphene electrodes, Chem. Sci. 6 (2015) 1996–2001.
[10] S. Iijima, Helical microtubules of graphitic carbon, Nature 354 (1991) 56–58.
[11] H.Y. Guan, C.L. Shao, S.B. Wen, B. Chen, J. Gong, X.H. Yang, A novel method for preparing Co_3O_4 nanofibers by using electrospun. PVA/cobalt acetate composite fibers as precursor, Mater. Chem. Phys. 82 (2003) 1002–1006.
[12] Y.Y. Gao, S.L. Chen, D.X. Cao, G.L. Wang, J.L. Yin, Electrochemical capacitance of Co_3O_4 nanowire arrays supported on nickel foam, J. Power Sources 195 (2010) 1757–1760.
[13] W.J. Zhou, J. Zhang, T. Xue, D.D. Zhao, H.L. Li, Electrodeposition of ordered mesoporous cobalt hydroxide film from lyotropic liquid crystal media for electrochemical capacitorsJ, Mater. Chem. 18 (2008) 905–910.
[14] L. Li, Y. Li, S.Y. Gao, N. Koshizaki, Ordered Co_3O_4 hierarchical nanorod arrays: tunable superhydrophilicity without UV irradiation and transition to superhydrophobicity, J. Mater. Chem. 19 (2009) 8366–8371.
[15] Y. Ding, Y. Liu, J. Parisi, L. Zhang, Y. Lei, A novel NiO–Au hybrid nanobelts based sensor for sensitive and selective glucose detection, Biosens. Bioelectron. 28 (2011) 393–398.
[16] T. Marimuthu, S. Mohamad, Y. Alias, Needle-like polypyrrole NiO composite for non-enzymatic detection of glucose, Synthetic Met. 207 (2015) 35–41.
[17] Y. Ding, Y. Liu, L. Zhang, Y. Wang, M. Bellagamba, J. Parisi, C.M. Li, Y. Lei, Sensitive and selective nonenzymatic glucose detection using functional NiO–Pt hybrid nanofibers, Electrochim. Acta 58 (2011) 209–214.
[18] A. Cao, J. Hu, H. Liang, W. Song, L. Wan, X. He, X. Gao, S. Xia, Hierarchically structured cobalt oxide (Co_3O_4): the morphology control and its potential in sensors, J. Phys. Chem. B 110 (2006) 15858–15863.
[19] L. Zheng, J. Zhang, J. Song, Ni(II)–quercetin complex modified multiwall carbon nanotube ionic liquid paste electrode and its electrocatalytic activity toward the oxidation of glucose, Electrochim. Acta 54 (2009) 4559–4565.
[20] W.H. Mulder, J.H. Sluyters, T. Pajkossy, I. Nyikos, Tafel current at fractal electrodes: connection with admittance spectra, J. Electroanal. Chem. 285 (1990) 103–115.
[21] Y. Mu, D. Jia, Y. He, Y. Miao, H. Wu, Nano nickel oxide modified non-enzymatic glucose sensors with enhanced sensitivity through an electrochemical process strategy at high potential, Biosens. Bioelectron. 26 (2011) 2948–2952.
[22] G. Wang, X. He, L. Wang, A. Gu, Y. Huang, B. Fang, B. Geng, X. Zhang, Non-enzymatic electrochemical sensing of glucose, Microchim. Acta 180 (2013) 161–186.
[23] T. Chen, X. Li, C. Qiu, W. Zhu, H. Ma, S. Chen, O. Meng, Electrochemical sensing of glucose by carbon cloth-supported Co_3O_4/PbO_2 core–shell nanorod, Biosens. Bioelectron. 53 (2014) 200–206.
[24] C. Xiang, Y. Zou, L.X. Sun, F. Xu, Direct electrochemistry and electrocatalysis of cytochrome *c* immobilized on gold nanoparticles–chitosan–carbon nanotubes-modified electrode, Talanta 74 (2007) 206–211.
[25] E. Kathryn, R.G. Toghill, Compton, Electrochemical Non-enzymatic Glucose Sensors: A Perspective and an Evaluation, Int. J. Electrochem. Sci. 5 (2010) 1246–1301.
[26] C.G. Zoski, Handbook of Electrochemistry, Elsevier Science, 2007 440.
[27] X. Zhang, A. Gu, G. Wang, Y. Huang, H. Ji, B. Fang, Porous Cu–NiO modified glass carbon electrode enhanced nonenzymatic glucose electrochemical sensors, Analyst 136 (2011) 5175–5180.
[28] X. Peng, W. Li, X. Liu, P. Hua, Electrodeposition of NiO_x/PANI composite film and its catalytic properties towards electrooxidations of polyhydroxyl compounds, J. Appl. Polym. Sci. 105 (2007) 2260–2264.
[29] W. Lian, L. Wang, Y. Song, H. Yuan, S. Zhao, P. Li, L. Chen, A hydrogen peroxide sensor based on electrochemically roughened silver electrodes, Electrochim. Acta 54 (2009) 4334–4339.
[30] A. Salimi, E. Sharifi, A. Noorbakhsh, S. Soltanian, Direct electrochemistry and electrocatalytic activity of catalase immobilized onto electrodeposited nano-scale islands of nickel oxide, Biophys. Chem. 125 (2007) 540–548.
[31] A. Safavi, N. Maleki, E. Farjami, Fabrication of glucose sensor based on a novel nanocomposite electrode, Biosens Bioelectron 24 (2009) 1655–1660.
[32] Y. Ding, Y. Wang, L. Su, H. Zhang, Y. Lei, Preparation and characterization of NiO–Ag nanofibers, NiO nanofibers, and porous Ag: towards the development of a highly sensitive and selective non-enzymatic glucose sensor, *J. Mater. Chem.* 20 (2010) 9918–9926.
[33] Y. Zheng, P. Li, H. Li, S. Chen, Controllable growth of cobalt oxide nanoparticles on reduced graphene oxide and its application for highly sensitive glucose sensor, Int. J. Electrochem. Sci. 9 (2014) 7369–7381.

[34] R. Ojani, J.-B. Raoof, B. Norouzi, Performance of glucose electrooxidation on Ni–Co composition dispersed on the poly(isonicotinic acid) (SDS) film, J. Solid State Electrochem. 15 (2011) 1139–1147.
[35] V.A. Kumary, T.E.M. Nancy, J. Divya, K. Sreevalsan, Nonenzymatic glucose sensor: glassy carbon electrode modified with graphene–nickel/nickel oxide composite, Int. J. Electrochem. Sci. 8 (2013) 2220–2228.
[36] S. Ci, T. Huang, Z. Wen, S. Cui, S. Mao, D.A. Steeber, J. Chen, Nickel oxide hollow microsphere for non-enzyme glucose detection, Biosens. Bioelectron. 54 (2014) 251–257.
[37] L. Wang, Y. Xie, C. Wei, X. Lu, X. Li, Y. Song, Hierarchical NiO superstructures/foam Ni electrode derived from Ni metal-organic framework flakes on foam Ni for glucose sensing, Electrochim. Acta 174 (2015) 846–852.